

Article

# Sloshing Response of an Aquaculture Vessel: An Experimental Study

Yanwu Tao <sup>1</sup>, Renqing Zhu <sup>1,\*</sup>, Jiayang Gu <sup>2</sup>, Qi Wei <sup>1</sup>, Fangxin Hu <sup>1</sup>, Xiaosen Xu <sup>2</sup>, Zhongyu Zhang <sup>2</sup> and Zhiyu Li <sup>3</sup>

<sup>1</sup> School of Naval Architecture and Ocean Engineering, Jiangsu University of Science and Technology, Zhenjiang 212003, China; tywkd@126.com (Y.T.)

<sup>2</sup> Marine Equipment and Technology Institute, Jiangsu University of Science and Technology, Zhenjiang 212003, China

<sup>3</sup> Marine Design & Research Institute of China, Shanghai 200023, China

\* Correspondence: zjczyzrq@163.com

**Abstract:** The sloshing response is crucial to the design and operation of aquaculture vessels and affects the safety of the culture equipment and the efficiency of the culture operation. A 1/50 scaled model was utilized to investigate the coupled sloshing response characteristics of a novel aquaculture vessel in a wave basin. Two wave directions (beam and head wave) and two filling levels (81.5% and 47.4%) are taken into account. The time-domain and frequency-domain characteristics of the sloshing response under the linear regular wave and extreme operational sea state were investigated using regular wave tests and irregular wave tests, respectively. The sloshing mechanism in the aquaculture tanks is complicated, due to the coupling effect between external waves, ship motion, and internal sloshing. In linear regular waves, the wave frequency mode dominates the sloshing response, which is larger under beam wave conditions than under head wave conditions and larger under half load conditions than full load conditions. The irregular wave test results confirmed the regular wave test conclusions, but the sloshing response has stronger nonlinearity, higher natural modes appeared, and the amplitude of the higher natural modes is also relatively larger.

**Keywords:** aquaculture vessel; model test; sloshing; coupling effect; higher natural mode; regular wave; irregular wave



**Citation:** Tao, Y.; Zhu, R.; Gu, J.; Wei, Q.; Hu, F.; Xu, X.; Zhang, Z.; Li, Z. Sloshing Response of an Aquaculture Vessel: An Experimental Study. *J. Mar. Sci. Eng.* **2023**, *11*, 2122. <https://doi.org/10.3390/jmse11112122>

Academic Editor: Spyros A. Mavrakos

Received: 7 October 2023

Revised: 26 October 2023

Accepted: 2 November 2023

Published: 6 November 2023



**Copyright:** © 2023 by the authors. Licensee MDPI, Basel, Switzerland. This article is an open access article distributed under the terms and conditions of the Creative Commons Attribution (CC BY) license (<https://creativecommons.org/licenses/by/4.0/>).

## 1. Introduction

With wild fish catches already approaching their maximum and human demand for mariculture increasing [1], mariculture production has more than doubled in the last 20 years and is predicted to more than double again in the next 30 years [2]. New farming techniques are needed to achieve sustainable aquaculture development. Researchers have proposed various forms of offshore aquaculture equipment concepts, including improved versions of traditional net pens [3], offshore closed aquaculture systems [4], ship-like structures [5], as well as integration on multi-purpose platforms [6], and energy production units. In these concepts, offshore closed aquaculture systems can improve the culture efficiency by controlling the culture environment (water temperature, NO<sub>x</sub>, etc.), isolating parasites and reducing environmental impacts through excreta and bait residue filtering. A novel form of farm vessel for deep-sea aquaculture with numerous closed aquaculture tanks is being developed and promoted by Chinese researchers [7]. The vessel has a total aquaculture volume of 100,000 m<sup>3</sup> and is able to sail autonomously to adapt to the harsher sea environment.

In harsh seas, violent sloshing responses may occur in the aquaculture tanks of aquaculture vessels. Severe sloshing will affect the cultural operations in the tanks, as well as the fish's growth and survival. In comparison to ordinary liquid cargo ships, aquaculture vessels must pay more attention to the sloshing problem, and there is minimal literature on the subject. The sloshing problem is a classical issue in the fields of both land and

sea liquid transport shipping, storage, and aerospace, and it has been intensively and extensively studied by a large number of scholars [8]. The study of the sloshing problem is mainly based on the theoretical method based on the potential flow theory [9], the experimental method based on the scaled model [10,11], and the numerical method based on RANS [12,13], MPS [14,15], and SPH [16], etc. For the aquaculture vessel with closed tanks, the coupling effect of hull motion and sloshing as well as the sloshing suppression methods are of qualitative concern.

The theoretical analysis of the problem of the coupled action of hull motion and sloshing is mostly solved by separating the internal and external domains, in which the external domain of the hull is solved by the linear potential flow theory, and the internal liquid tank domain is dealt with by two methods: one is based on the viscous method of calculating the sloshing loads based on the viscous method such as the linear potential flow method [17–19], the multimodal method [20], the finite difference method [21], and the fourth-order Runge–Kutta method [22], and the other one is based on the viscous method [23–25]. With the development of computer technology and computational fluid dynamics, scholars have widely adopted the RANS method to calculate the sloshing in the liquid tanks and the coupling between the hull's motion and the liquid tanks [26,27]. For experimental studies, Zhao et al. [28] investigated the response of a single liquid tank under the white noise wave. Kim et al. [29] and Zhao et al. [30] conducted tests on ships with two tanks arranged fore and aft, and Igbadumhe et al. [31] and Li et al. [32] investigated the coupled motions and the sloshing response of an FPSO and an aquaculture vessel with left and right double rows of tank arrangements.

Although the sloshing effect can be used on the anti-roll tanks [33] and tuned liquid damper [34] to improve the motion performance, the sloshing effect is more noteworthy for its adverse effects on the free surface's stability and the impact load on the structure. To suppress the sloshing response, scholars have designed various methods to decrease the free surface area or utilize obstacles to dissipate the kinetic energy of inner water [35], such as arranging trusses and protruding structures on the bulkhead [36], or fitting fixed [37] or floating [38,39] horizontal or vertical structures inside the tanks. These sloshing suppression methods are widely used on conventional vessels, but these protruding structures may affect fishing operations and even cause potential fish damage. Considering the suitability for fishing, some scholars have explored the sloshing suppression method in aquaculture vessels. Cui et al. [40] studied the sloshing response of an aquaculture tank with an inclined top using a numerical simulation, and Gao et al. [41] investigated the sloshing effect of arranging intermittent vertical cylinders and continuous vertical flat plates on the top of the tank and the effect on the velocity field. Wiegerink et al. [42] designed an annular sloshing suppression structure with a rectangular cross-section for a cylindrical closed aquaculture platform and validated its suppression effect by experimental and numerical methods.

This paper focuses on analyzing the sloshing response of a novel aquaculture vessel using the experimental method, and it is structured as follows. In Section 2, the model test scheme and the calibration of the sensors are described. In Section 3, the frequency-domain sloshing response characteristics under linear regular waves are investigated. The wave frequency mode and higher natural mode of the sloshing response are identified, and the effects of the position of the aquaculture tank and the walkway on the sloshing response are analyzed. In Section 4, the complex sloshing response under extreme operating conditions is analyzed based on irregular wave tests.

## 2. Vessel Description and Experimental Setup

The design operation area of the aquaculture vessel is the Yellow Sea and South China Sea of China, and the design operation depth is 100 m–500 m. The aquaculture vessel is designed to extract deep water and maintain the proper flow speed and temperature in the tanks by the recirculating water systems for the culture of Atlantic salmon and *pseudosciaena crocea*. The aquaculture vessel has a two-propeller propulsion system that allows it to cruise autonomously or relocate during typhoons. To investigate the

hydrodynamic and sloshing performance of the aquaculture vessel, model tests at a scale ( $\lambda$ ) of 1:50 were carried out.

2.1. Description of the Vessel

The aquaculture vessel is arranged in a double row of tanks, with longitudinal and transverse bulkheads separating the hull into several near-square aquaculture tanks. The side view of the main hull is shown in Figure 1. Aquaculture tanks No.1 to No.14 (in Figure 1) are standard tanks with an aquaculture volume of 5300 m<sup>3</sup>, and No.15 to No.18 are non-standard tanks. Compared with the conventional liquid carriers, the aquaculture vessel has more aquaculture tanks, the longitudinal and transverse dimensions of the aquaculture tanks are close to each other, and small equipment cabins are arranged at the transverse and longitudinal intervals of the aquaculture tanks. Economically, the construction cost of an aquaculture vessel is close to that of a conventional liquid cargo vessel of the same displacement. The main particulars of the vessel are presented in Table 1.

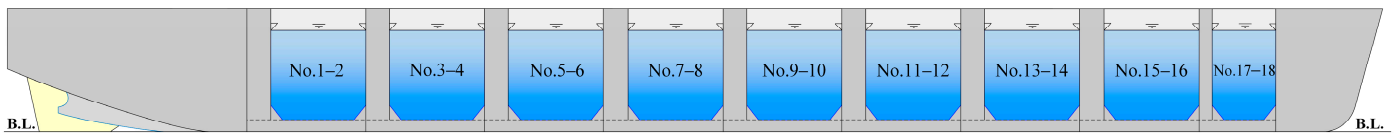


Figure 1. Side view of the aquaculture vessel.

Table 1. Main particulars of the aquaculture vessel.

Designation	Signal	Unit	Value	
			Full Scale	Model
Length overall	$L_{OA}$	m	258.20	5.164
Length between perpendiculars	$L_{PP}$	m	250.56	5.011
Breadth	$B$	m	44.00	0.880
Depth	$D$	m	22.80	0.456

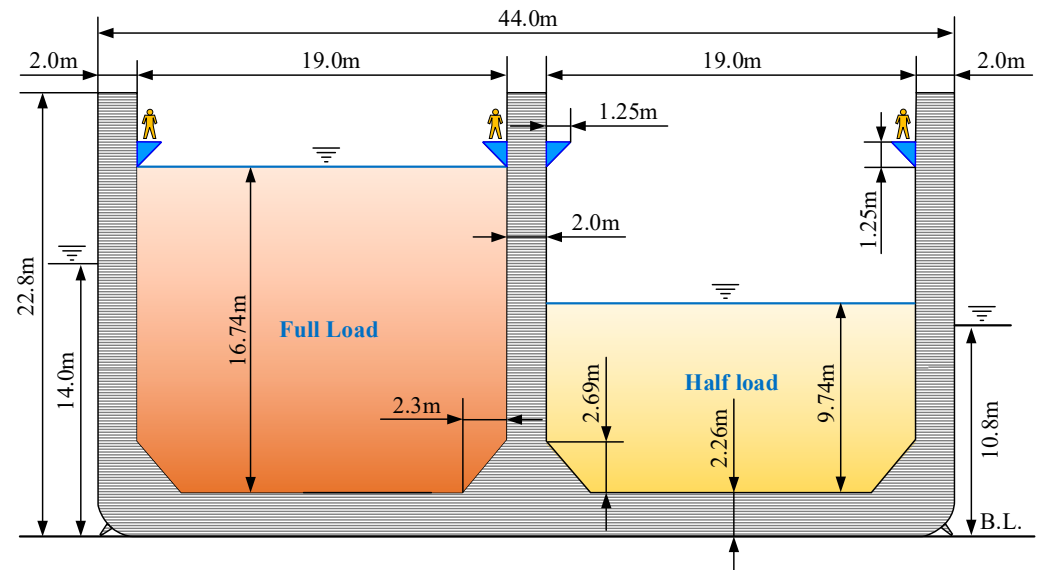
The aquaculture vessel consists of two typical loading conditions, full load and half load, which correspond to a filling level (water depth/tank height) of 81.5% and 47.4% in the aquaculture tanks, respectively. Since sufficient space needs to be retained in the upper part of the aquaculture tanks for personnel operations, the design full load condition of the aquaculture vessel has a lower filling level than that defined for a conventional liquid cargo vessel (95% or more). The mass and moment of inertia parameters of the vessel for the two filling levels are shown in Table 2.

Table 2. Mass and moment of inertia parameters [43].

Designation	Signal	Unit	Full Load		Half Load	
			Full Scale	Model	Full Scale	Model
Draft	$d$	m	14.00	0.28	10.80	0.216
Displacement	$\Delta$	t	138,971	1.085	105,326	0.822
Center of gravity above BL	$V_{CG}$	m	11.78	0.236	10.34	0.207
Center of gravity from AP	$L_{CG}$	m	125.31	2.506	126.01	2.520
Roll radius of gyration	$k_{xx}$	m	13.68	0.274	14.39	0.288
Pitch radius of gyration	$k_{yy}$	m	61.53	1.231	64.84	1.297
Yaw radius of gyration	$k_{zz}$	m	62.33	1.247	65.63	1.313

The aquaculture tanks have chamfers on the bottom and side walls, and the vertical walls are fitted with walkways to enable personnel culture operation inside the tanks. The transverse section of the vessel at a standard aquaculture tank is shown in Figure 2.

The standard tanks have a width of 19.0 m, a length of 17.84 m, and a water depth of 16.74 m for the full load condition and 9.74 m for the half load condition, respectively. The depth-to-length ratio ( $h/l$ ) of the aquaculture tank, i.e., the ratio of the water depth ( $h$ ) to the length in the sloshing direction ( $l$ ), is an important factor affecting the sloshing characteristics. For transverse sloshing, the  $h/l$  was 0.51 and 0.89 for full load and half load conditions, respectively; for longitudinal sloshing, it was 0.55 and 0.95 for full load and half load conditions.



**Figure 2.** Transverse section of the aquaculture vessel at a standard aquaculture tank.

### 2.2. Facility and Test Model

Model tests were performed in the Special Vehicle Research Institute at the AVIC (Aviation Industry Corporation) of China. The basin has an overall length of 60 m, width of 60 m, and depth of 5 m. The wave generators are capable of making waves with wavelengths ranging from 0.5 m to 15 m, wave heights between 0.05 m and 0.5 m, and maximum significant wave heights of 0.3 m for long-crested irregular waves. The main body of the aquaculture vessel model is composed of multi-layer board and fiber reinforced plastics, and the internal aquaculture tanks are made of 6 mm thick plexiglass. The aquaculture vessel model and inner tankers are shown in Figures 3 and 4. The support structure is specially designed to maintain the counterweight block in the test, and the position of the counterweight unit can be precisely modulated by screws. The model geometric tolerances and mass distribution have been verified in the previous work [43], which satisfies the requirements of the ITTC Recommended Procedures and Guidelines [44].



**Figure 3.** Aquaculture vessel model in the basin.

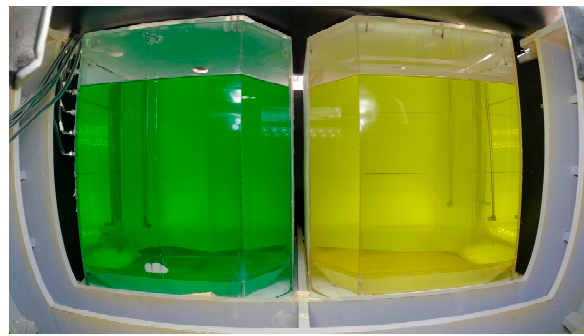


**Figure 4.** Aquaculture tank model.

Four horizontal mooring cables consisting of soft springs and thin wire ropes were used to prevent the model from drifting off. The stiffness of the spring is 88 N/m, and the pre-tension is 45 N. The cable does not slacken during testing, and the natural period of the surge and sway motion caused by the mooring cables is much larger than the natural period of the wave frequency motion (heave, roll, and pitch). A single anchor chain mooring is used for the aquaculture vessel during the aquaculture operation, which has instability in beam wave conditions. To study the extreme sloshing response of the aquaculture vessel under the beam wave, the same mooring arrangement is still used for the irregular wave test.

### 2.3. Sensor Arrangement and Calibration

In the model test, a set of gyroscope units was installed at the hull’s center of gravity to measure the roll and pitch motion; a mini camera was installed in the open space at the stern of the hull to record the sloshing phenomenon of the aft aquaculture tanks (No.1 and No.2); and 10 wave gauges (WG) were set up at multiple aquaculture tanks to measure the wave elevation in the typical position. The arrangement of the camera and all the sensors is shown in Figure 5.

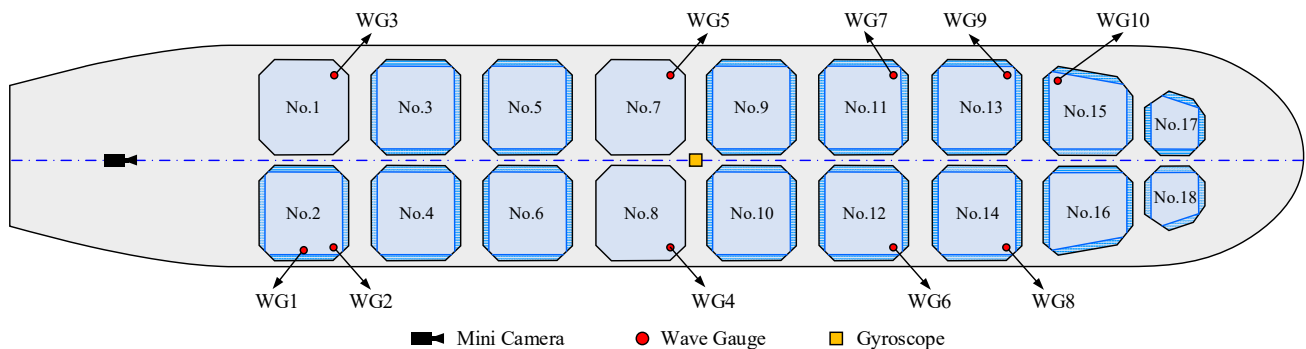


**Figure 5.** Arrangement of the camera and all the sensors.

The wave gauge WG1–WG3 arrangement at the hull stern is shown in Figure 6. The still free surface of the aquaculture tank under full load conditions was at the lower edge of the inclined brace plate of the walkway. To reduce the impact of the walkway on the sensors, the capacitance filaments of the wave gauges were placed at a specific distance from the walkway’s outer edge, and all wave gauges were placed at a distance ( $d_1$  in Figure 6) of 3.5 cm from the tank walls they were closest to. Therefore, at full scale, the distances from WG1 and WG2 to the center of the aquaculture tank are 7.75 m and 6.67 m, respectively. Tank No.1 in the stern, as well as Nos. 7 and 8 in the amidships, does not install the walkway and aims to evaluate the sloshing response unaffected by the walkway. WG1 is situated in the center of the aquaculture tank’s sidewall and mainly measures the pure transverse sloshing response; the remaining WGs are located at the aquaculture tanks’ corners and can measure both longitudinal and transverse sloshing responses.

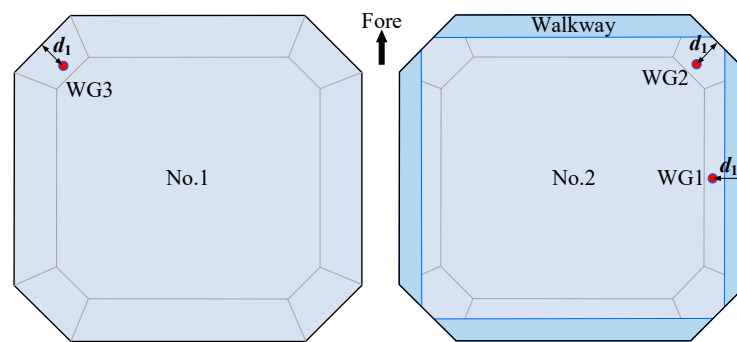


**Figure 6.** Arrangement of WG1–WG3 at the hull stern.

The wave gauge has a range of 50 cm and a sampling frequency of 100 Hz, with an accuracy of 0.15%. Before the model test, the acquisition unit and gyroscope system are calibrated at a special testing institution. The gyroscope system is sampled at 1.25 kHz. The camera records at a frame rate of 60 fps and 4 K resolution. The parameters and accuracy of the main sensors are summarized in Table 3.

**Table 3.** Parameters and accuracy of main sensors.

Instrument	Sensor Type	Measuring Range	Accuracy
Data acquisition unit	PCM-006	0–5 V	0.01 V
Gyroscope	IMU610H	−90°–90°	0.05°
Wave gauge	YWH200-D	50cm	0.15%
Electronic hanging scale	OCS-3T	2000 kg	0.5 kg
Electronic platform scale	MTC002C	100 kg	0.01 kg

### 3. Sloshing Response under Regular Waves

When a regular wave test is used for the study, the wave parameters should consider the coupling effect between the external wave, hull motion, and internal sloshing. In this chapter, the parameters of the regular waves (Section 3.1) are first determined considering the aquaculture tanks’ natural sloshing properties, as well as the motion performance of the vessel and the basin’s wave-making capacity. Following that, the sloshing response under the beam wave and head wave is studied. Due to the significant difference in the magnitude of the sloshing response for the two wave headings, the beam wave condition (Section 3.2) and the head wave condition (Section 3.3) are investigated independently.

#### 3.1. Regular Wave Parameters

If the chamfers on the bottom and sides of the aquaculture tank are neglected and the tank can be considered as a cuboid, then its  $n$ -th natural period of sloshing response can be given by the formula

$$T_n = \frac{2\pi}{\sqrt{n\pi g \tanh(n\pi h/l)}/l}, n= 1, 2, 3, \dots \tag{1}$$

where  $T_n$  is the  $n$ -th natural period,  $g$  is the gravity acceleration,  $h$  is the water depth, and  $l$  is the width of the tank, respectively. The first four natural frequencies and periods of transverse and longitudinal sloshing at full scale are shown in Table 4. The  $n$ -th natural frequencies of transverse and longitudinal sloshing are denoted as  $f_{Tn}$  and  $f_{Ln}$ , and the  $n$ -th natural period of transverse and longitudinal sloshing are denoted as  $T_{Tn}$  and  $T_{Ln}$ , respectively. It can be seen that the first four natural periods of the sloshing range from 2.39 s to 4.95 s.

**Table 4.** Theoretical natural frequencies and periods of sloshing in full scale.

Mode Order $n$	Load Condition	Transverse Sloshing		Longitudinal Sloshing	
		Frequency $f_{Tn}$ (Hz)	Period $T_{Tn}$ (s)	Frequency $f_{Ln}$ (Hz)	Period $T_{Ln}$ (s)
1	Full load	0.202	4.953	0.209	4.794
	Half load	0.195	5.134	0.203	4.938
2	Full load	0.287	3.489	0.296	3.380
	Half load	0.286	3.494	0.296	3.384
3	Full load	0.351	2.848	0.362	2.760
	Half load				
4	Full load	0.405	2.467	0.418	2.390
	Half load				

The wavelength range of the regular wave should be at least  $0.5 L_{pp}$  to  $2.0 L_{pp}$ , and the wave steepness should be around  $1/50$ , according to the ITTC method [45]. The minimum wave height of the wavemaker for regular waves is 0.05 m. If the wave period is close to the sloshing natural period, the wave steepness must be less than  $1/15$ , and the wavemaker cannot generate continuous waves with a specified period and wave height. Combining factors such as the basin’s wave-making capacity and model scale, the wave height of the regular wave was finally chosen as 50 mm, the wavelength range was 2 m–10.125 m, the wavelength to vessel length ratio was 0.4–2.025, and the corresponding wave period was 8 s–18 s at full scale. The wave parameters of the regular wave test are shown in Table 5.

**Table 5.** Wave parameters of regular wave model test.

Model.			Full Scale		$\lambda_w/L_{pp}$	$H/\lambda_w$
$H_m$ (m)	$\lambda_m$ (m)	$T_m$ (s)	$\lambda_s$ (m)	$T_s$ (s)		
0.05	2.000	1.131	100.00	8.0	0.400	1/40
	3.125	1.414	156.30	10.0	0.625	1/63
	3.781	1.556	189.06	11.0	0.756	1/76
	4.500	1.697	225.00	12.0	0.900	1/90
	4.883	1.768	244.14	12.5	0.977	1/98
	5.281	1.838	264.06	13.0	1.056	1/106
	6.125	1.980	306.25	14.0	1.225	1/123
	7.031	2.121	351.56	15.0	1.406	1/141
	8.000	2.263	400.00	16.0	1.600	1/160
	10.125	2.546	506.25	18.0	2.025	1/203

### 3.2. Beam Wave Condition

Since the vessel has multiple aquaculture tanks, the time history and spectral analyses of the sloshing response at typical locations were first performed, and then, the effects of location and walkways on localized sloshing were evaluated by considering the differences between the in-vessel and in-tank locations.

#### 3.2.1. Time and Frequency Domain Response

Based on the Froude scaling law [46], the conversion relations for the main physical quantities are shown in Table 6. The subscripts s and m denote the full scale and model scale, respectively.

**Table 6.** Froude scaling law for the involved physical quantities.

Physical Quantity	Model	Full Scale
Time	$t_m$	$t_s = t_m \sqrt{\lambda}$
Wave period	$T_m$	$T_s = T_m \sqrt{\lambda}$
Frequency	$f_m$	$f_s = f_m / \sqrt{\lambda}$
Sloshing amplitude	$\zeta_m$	$\zeta_s = \zeta_m \lambda$

The wave gauge WG1 mainly measures transverse sloshing and is less affected by longitudinal sloshing, so the data of WG1 was chosen as a typical sloshing response to analyze. The time history and response spectrum of the sloshing response at WG1 in the full load condition under beam waves is shown in Figure 7. The incident wave frequency ( $f_W$ ) is shown in Figure 7b as a red background region, and the first natural frequency ( $f_{T1}$ ) of transverse sloshing is shown as a gray background region. When the wave period is less than 14 s, the sloshing response time history is nearly sinusoidal, and the sloshing response is dominated by the wave frequency response. However, when the wave period is greater than or equal to 14 s, the sloshing response shows a specific higher natural mode, and the higher natural mode is mainly caused by the first natural mode. The truncation of the data has some effect on the peak position of the spectrum, combined with the wave period uncertainty during the model test, resulting in the peak period in the sloshing spectrum deviating from the theoretical value.

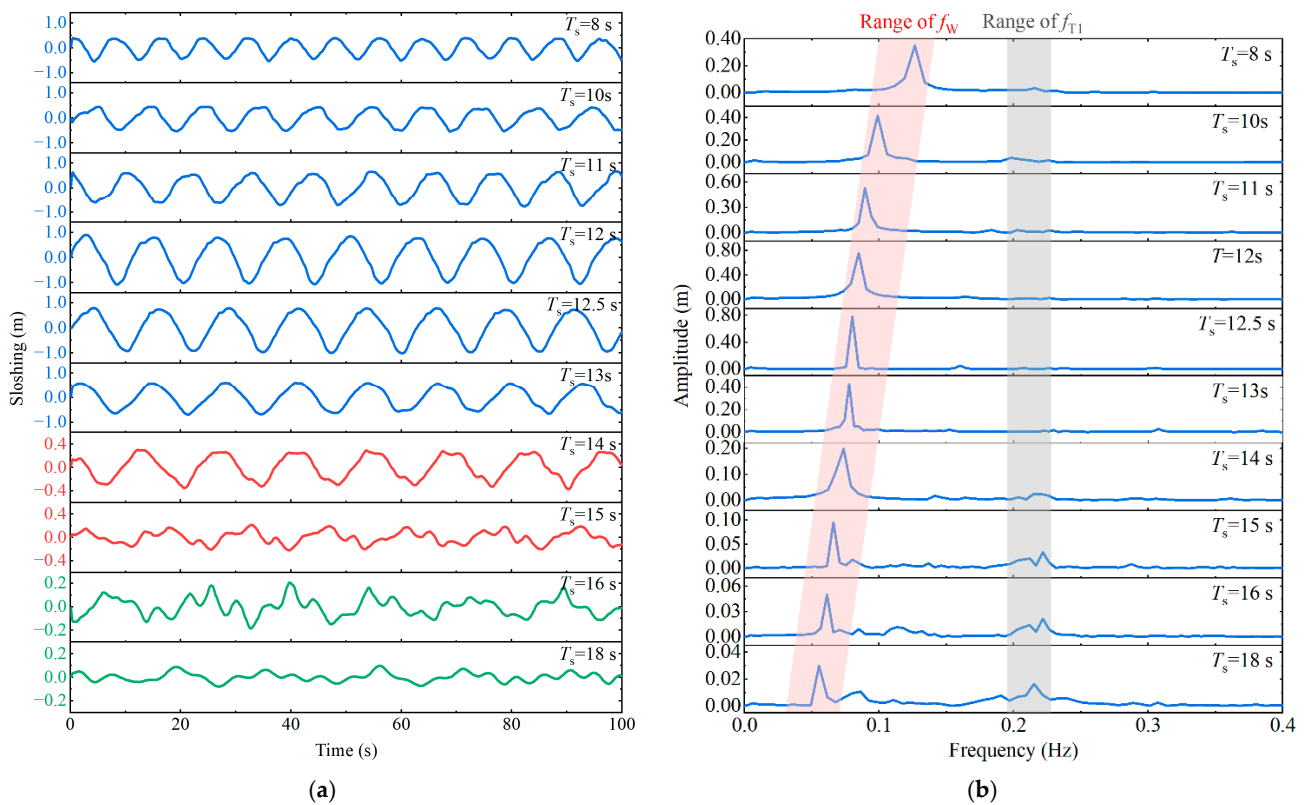


**Figure 7.** Sloshing time history and response spectrum under full load and regular beam wave condition. (a) Sloshing time history; (b) Response spectrum.

For data processing, the initial steady-state interval was intercepted for the sloshing responses of all wave gauges, and band-pass filtering was used to extract the sloshing responses corresponding to the different modes. The wave-frequency mode of the sloshing has a truncation frequency of  $0.9\text{--}1.1 f_W$ , and similarly, the first natural mode cutoff ranges from  $0.9$  to  $1.1 f_{T1}$ . The sloshing RAO is defined as the ratio of the sloshing amplitude to the wave height ( $H_m$ ) of the external incident wave. The sloshing RAOs of the wave frequency mode and the first natural mode of all wave gauges under the full load condition at beam sea are shown in Figure 8. The roll natural period at the full load condition is around 12.2 s. According to Figure 8a, the sloshing RAO of wave frequency mode reaches its maximum value when the wave period is close to the roll natural period. There are certain variances in the sloshing response at different wave gauges, and to represent the discretization of the sloshing RAOs in various wave gauges, the dimensionless standard deviation of the sloshing RAOs (denote as  $\hat{\sigma}(\text{RAO})$ ) is defined as the ratio of the RAOs' standard deviation

to their mean value for all wave gauges. When the wave period is smaller than 15 s, the  $\hat{\sigma}(\text{RAO})$  is smaller than 6%, and when the wave period is greater than or equal to 15 s, it ranges from 13.5% to 22.5%. Overall, when the wave period is close to the roll natural period, the  $\hat{\sigma}(\text{RAO})$  is minimized; from another perspective, the larger the sloshing RAO, the smaller its dimensionless dispersion. In Section 3.2.2, more details of the variations in sloshing response among the wave gauges are investigated.

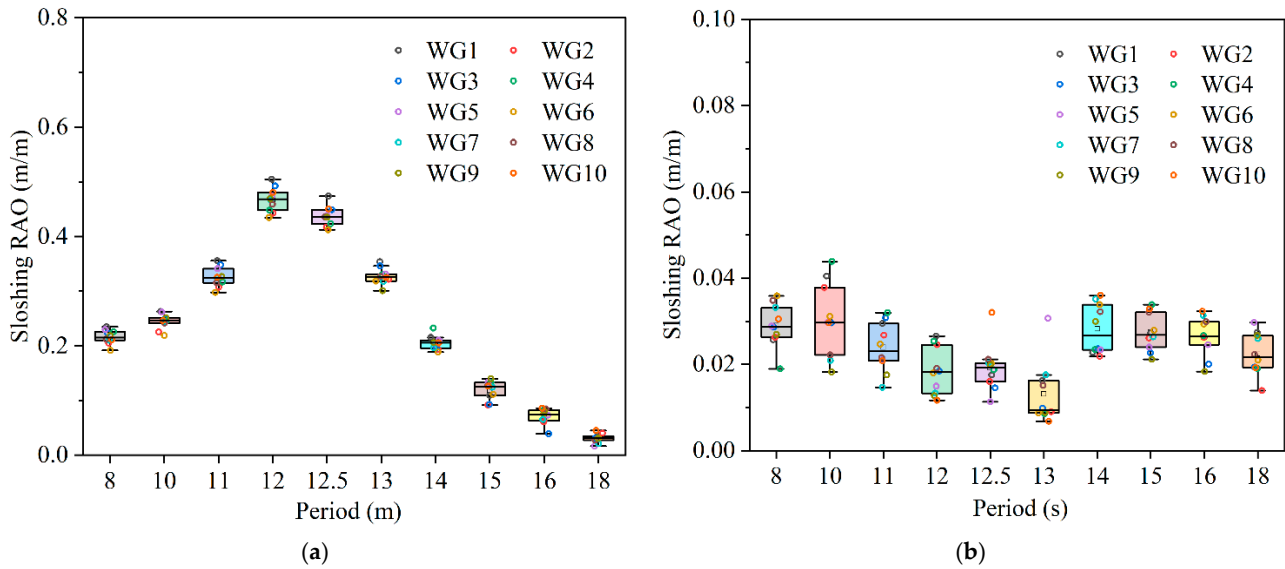


**Figure 8.** Sloshing RAOs under full load and beam wave condition. (a) Wave frequency mode; (b) First natural mode.

The first natural mode of the sloshing RAO has a smaller amplitude near the roll natural period (12 s–13 s). In particular, when the wave period is 10 s, the wave period is about twice the first natural period, and a larger first natural mode is excited. The ratio of the first natural mode to the wave frequency mode increases as the wave period shifts away from the roll natural period.

The time history and response spectrum of the sloshing response at WG1 in the half load condition under beam waves are shown in Figure 9. As can be seen from Figure 9a, the sloshing responses for all wave periods, except for wave periods of 8 s and 12 s, exhibit a distinct multi-frequency superposition mode, which can be confirmed by the sloshing response spectrum in Figure 9b. For all wave periods, the sloshing response showed a certain doubling frequency mode ( $2f_W$ ), especially at wave periods of 15 s–18 s, the ratio of the doubling frequency mode ( $2f_W$ ) to the wave frequency ( $f_W$ ) mode increased from 0.5 to 0.9. When the wave period is 10 s, it triggers a significant first natural frequency ( $f_{T1}$ ) mode, with an amplitude approximately twice that of the wave frequency mode. The first natural mode of the sloshing response is progressively larger than the wave frequency mode when the period is greater than or equal to 13 s.

The sloshing RAOs of the wave frequency mode and the first natural mode of all wave gauges under the half load condition at beam sea are shown in Figure 10. The roll natural period in the half load condition is around 11.6 s. From Figure 10a, it can be seen that the sloshing RAO of the wave frequency mode in the half load condition is maximum when the wave period is close to the roll natural period, which is similar to that of the full load condition. There is a certain variation in the sloshing RAO at different wave gauges, specifically, the  $\hat{\sigma}(\text{RAO})$  is less than 11% for wave periods shorter than 15 s, and 21.2–24.7% for wave periods of 15 s to 18 s.

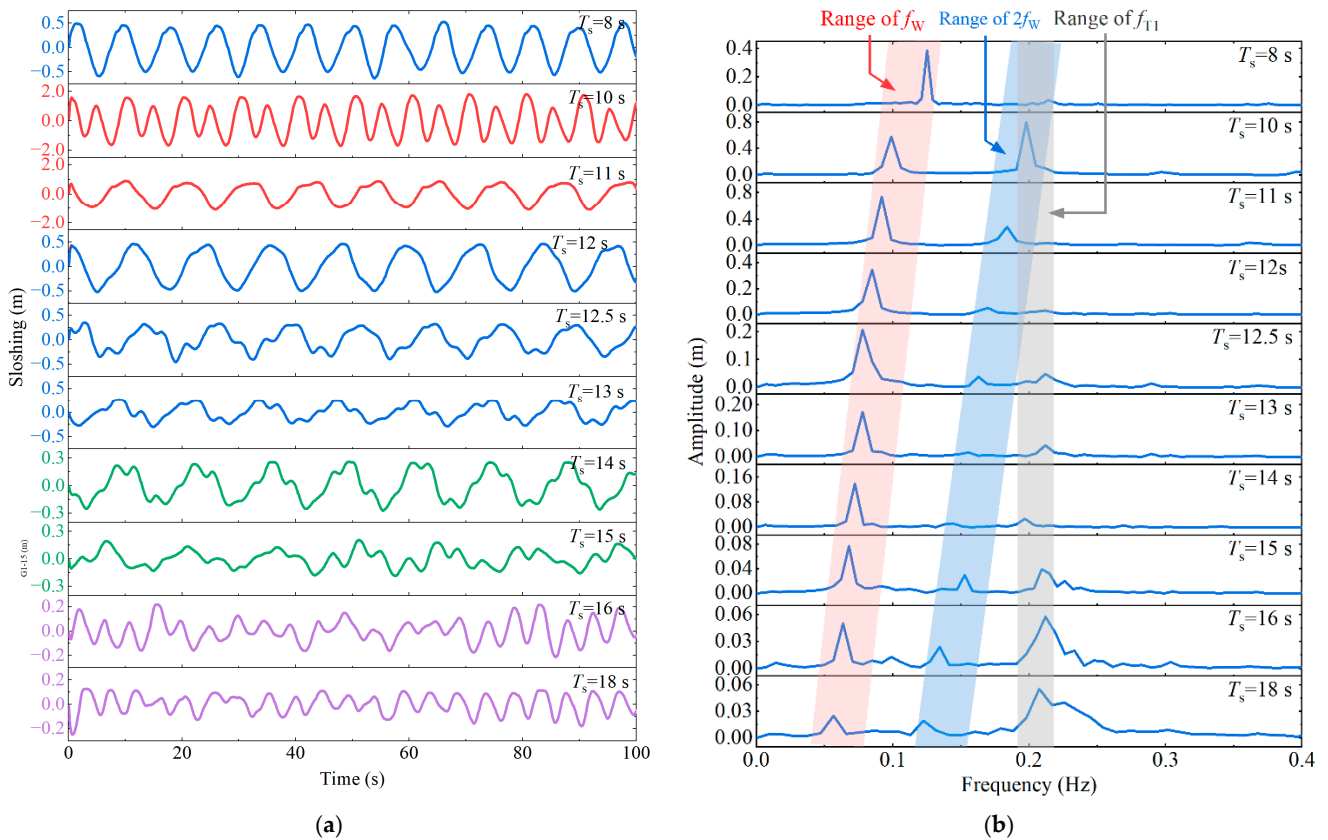


**Figure 9.** Slushing response and response spectrum under half load and regular beam wave condition. (a) Slushing time history; (b) Response spectrum.

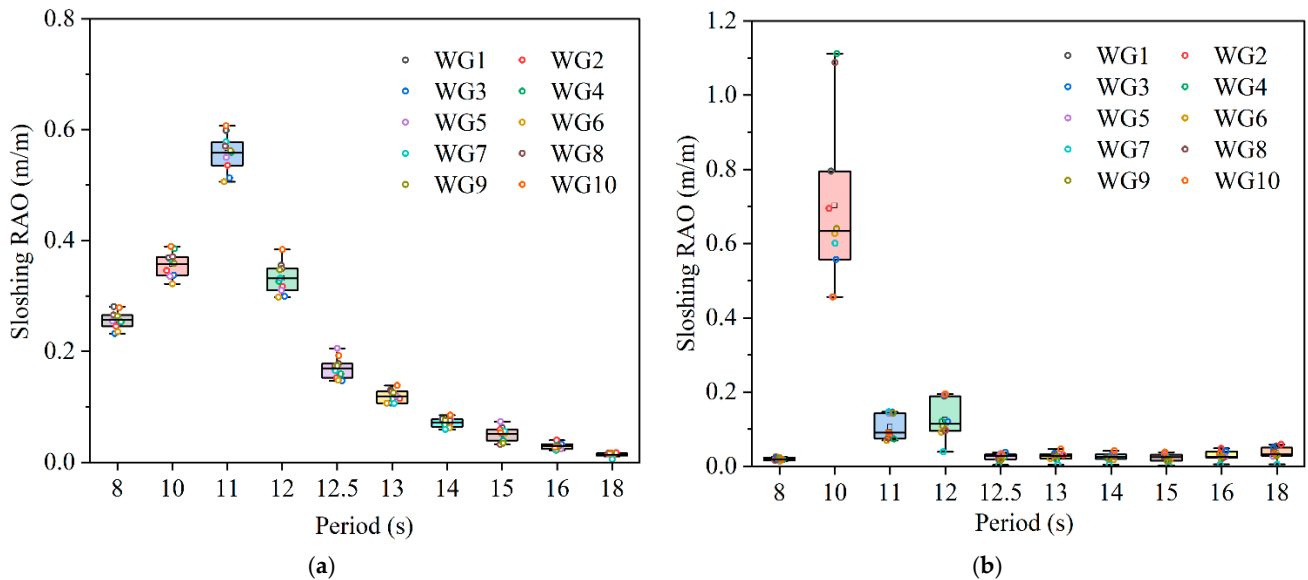


**Figure 10.** Slushing RAO under half load and beam wave condition. (a) Wave frequency mode; (b) First natural mode.

Figure 10b shows that the first natural mode with a wave period of 10 s is significant compared with other wave periods in the half load condition. The mean value of the first natural mode is close to 1.9 times that of the wave frequency mode, and close to 3 times at some wave gauges, which mainly resulted from the wave period being close to 2 times the first natural period. Except for wave periods around 10 s, both the first natural mode

( $f_{T1}$ ) and the doubling frequency mode ( $2f_W$ ) are larger under long-period waves ( $T_s \geq 15$  s) and their amplitudes are bigger than the wave frequency mode for some wave periods. Comparatively, for the beam wave condition, the wave frequency mode, the first natural mode, and the doubling frequency mode are larger in the half load condition than those in the full load condition.

### 3.2.2. The Effect of Tank Position and Walkway

Due to the various distances from each aquaculture tank to the center of the vessel, the acceleration of each tank varies somewhat, which may result in different sloshing responses in different aquaculture tanks. Furthermore, the aquaculture tanks are fitted with walkways, which can affect the free surface shape within the tank. In this section, the effect of the aquaculture tanks' location in the vessel and the location within the aquaculture tank on the sloshing are specifically investigated.

The vessel has a double-row arrangement of aquaculture tanks, with different longitudinal and transverse positions of the tanks in the hull. Figure 11 shows the sloshing response of the wave gauges at typical locations under full load conditions with a wave period of 12 s, and walkways are installed in all the aquaculture tanks where the wave gauges are installed. In particular, Figure 11a shows the sloshing response of three wave gauges (WG2, WG6, and WG8) at different longitudinal positions, and Figure 11b shows the sloshing response of wave gauges (WG8 and WG9) at different transverse positions. The sloshing amplitudes of WG2, WG6, and WG8 are 1.30 m, 1.28 m, and 1.36 m, respectively, and the relative difference at WG2 and WG8 is 6.2%. The sloshing amplitudes of WG8 and WG9 were 1.36 m and 1.39 m, respectively, with a relative difference of 2.2%.

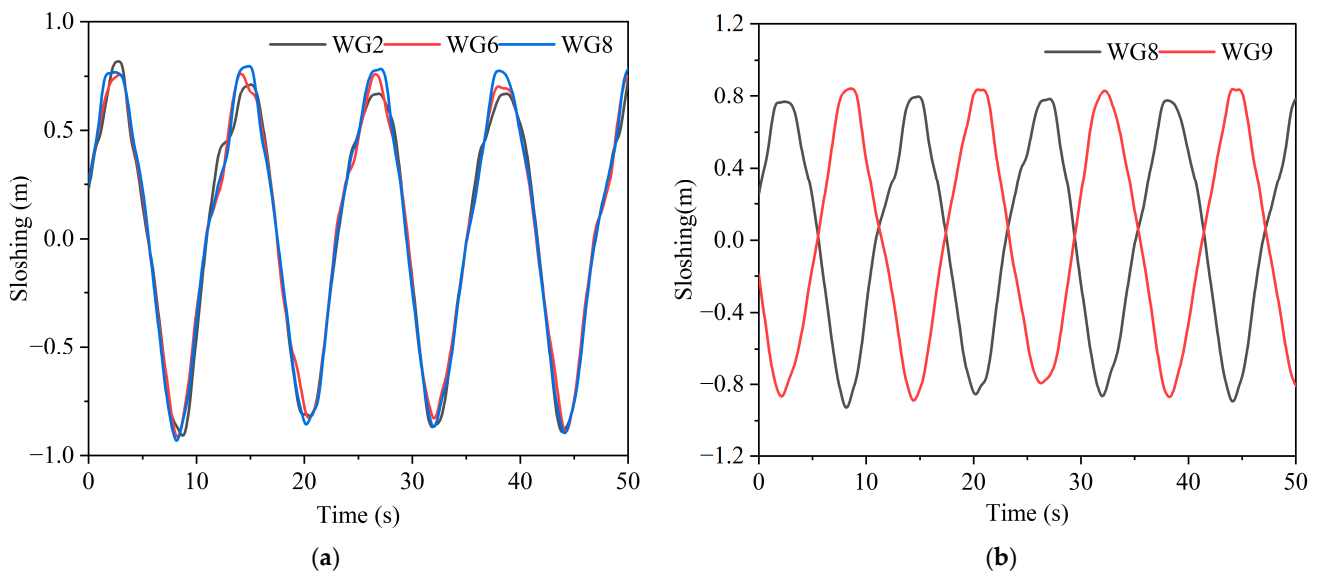


**Figure 11.** Sloshing response at different locations under full load condition. (a) Different longitudinal positions; (b) Different transverse positions.

Figure 12 shows the sloshing response of WG1 at the center of the side walkway and WG2 at the walkway connection in the tank No.2. The sloshing response amplitude of WG1 is 14.6% larger than that of WG2, and in addition, WG1 has a localized peak just before the maximum, which is caused by the reflective effect of the inclined brace plate of the walkway.

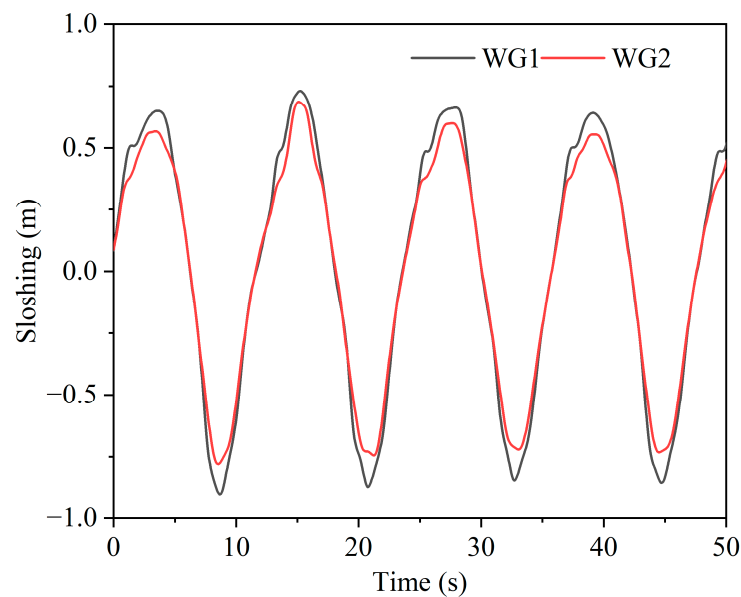


**Figure 12.** Sloshing response at different locations within the tank.

In general, the sloshing response of WG1 is about 15% larger than the other wave gauges in the beam wave condition, based on an analysis of the amplitudes of all the wave gauges. Meanwhile, the distribution of the sloshing amplitude at different wave height gauges shows a certain randomness, and the difference in sloshing response between the other wave gauges (WG2–WG10) is less than 10%.

### 3.3. Head Wave Condition

WG2 is located in the tank No.2 where the walkway is installed, and its longitudinal sloshing is representative; therefore, the sloshing response of WG2 is analyzed under head wave conditions. The time history and response spectrum of the sloshing response at WG2 in the full load condition under head waves are shown in Figure 13.

In the head wave condition, the sloshing response is dominated by the wave frequency mode for both loading conditions. As shown in Figure 13, the doubling frequency mode exists ( $2f_w$ ) when the wave period is 12 s–13 s for the full load condition, and the first natural mode occurs when the wave period is large ( $T_s = 15$  s–18 s). From Figure 14, it can be found that a significant doubling frequency mode ( $2f_w$ ) occurs in the half load condition, with periods of 10 s–12.5 s, while the first natural mode occurs at periods of 16 s–18 s. In contrast, for the same regular wave excitation, the sloshing amplitude in the head wave condition is smaller than that of the beam wave condition, and its nonlinearity is weaker likewise.

The sloshing RAOs of the wave frequency mode in the full load and half load conditions under the heading wave condition are shown in Figure 15. Since WG1 mainly measures the transverse sloshing, the sloshing response of this wave gauge is not analyzed in the head wave condition. Furthermore, several wave gauge data were removed since the sloshing amplitude in some wave periods was smaller than 1 mm, which causes challenges to the measurement and data processing. It can be seen that the sloshing RAO of the wave frequency mode for the full and half load conditions shows a maximum at the wave period of 11 s–13 s. The peak sloshing RAO in the head wave condition does not occur in the range of the pitch natural period. The sloshing response measured at the different wave gauges was relatively dispersive, with a  $\hat{\sigma}$ (RAO) of 31–47%, of which the dispersion was slightly larger for the half load condition than for the full load condition. In the regular wave tests, the longitudinal sloshing response in the head wave condition is at a small level, and its amplitude is about 1/10 of that of the corresponding beam wave condition, so the sloshing response at different tanks in the head wave condition was not analyzed specifically.

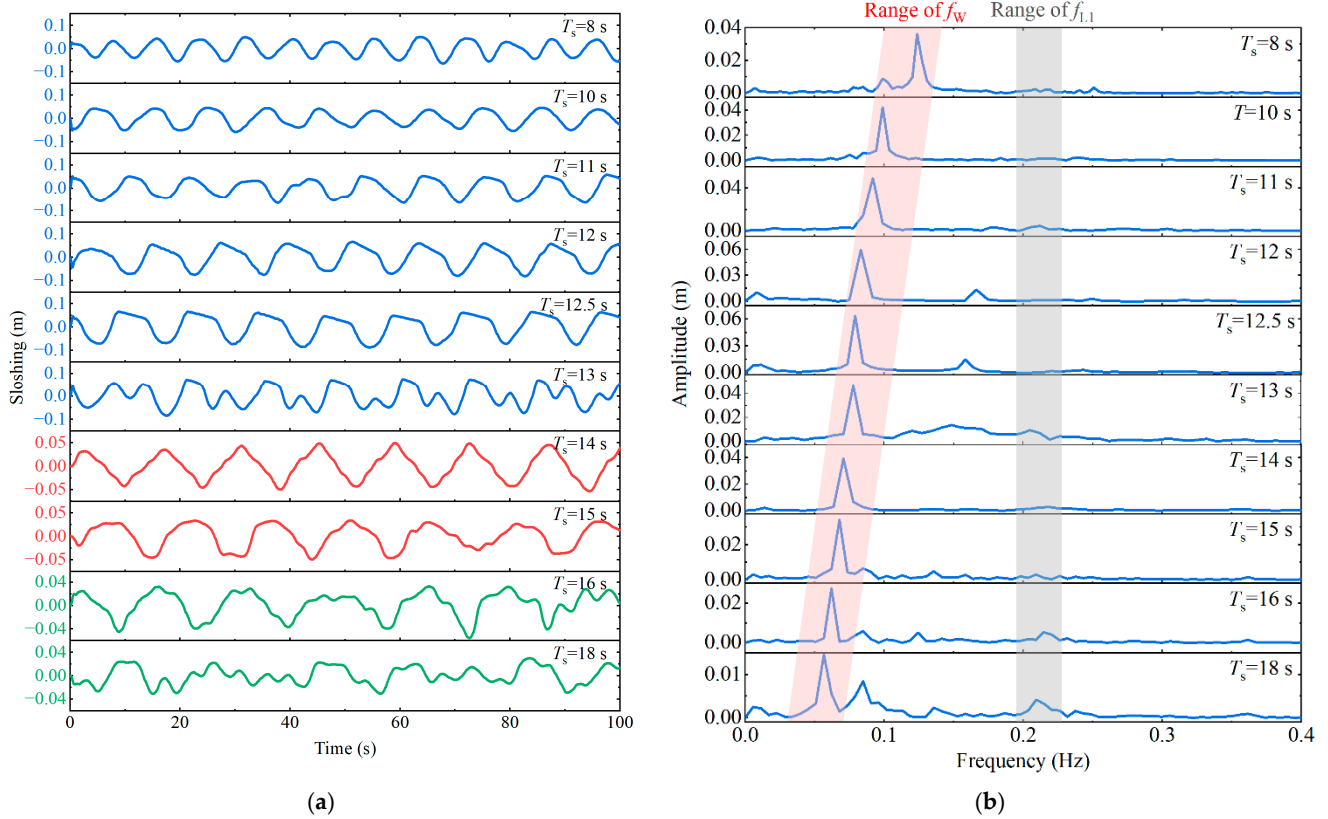


**Figure 13.** Slushing response and response spectrum under full load and regular head wave condition. (a) Slushing response; (b) Response spectrum.

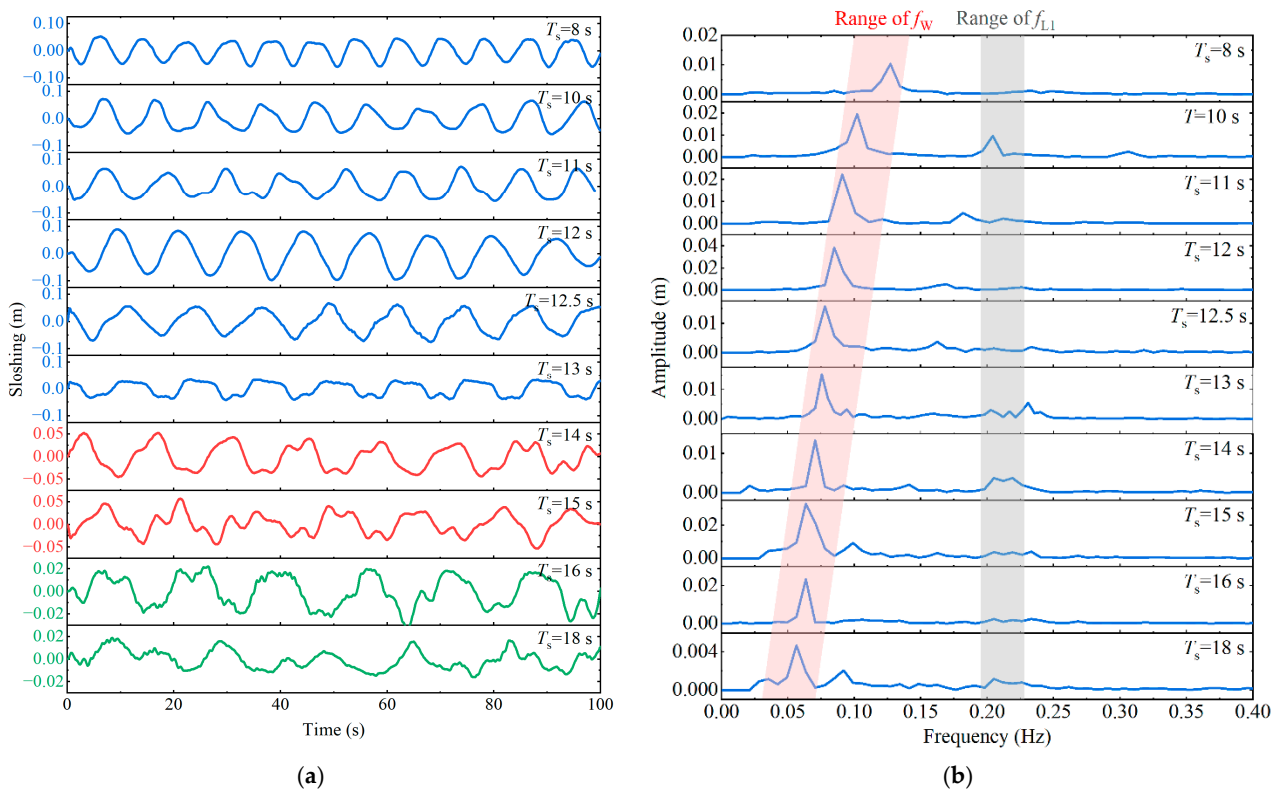


**Figure 14.** Slushing response and response spectrum under half load and regular head wave condition. (a) Slushing response; (b) Response spectrum.

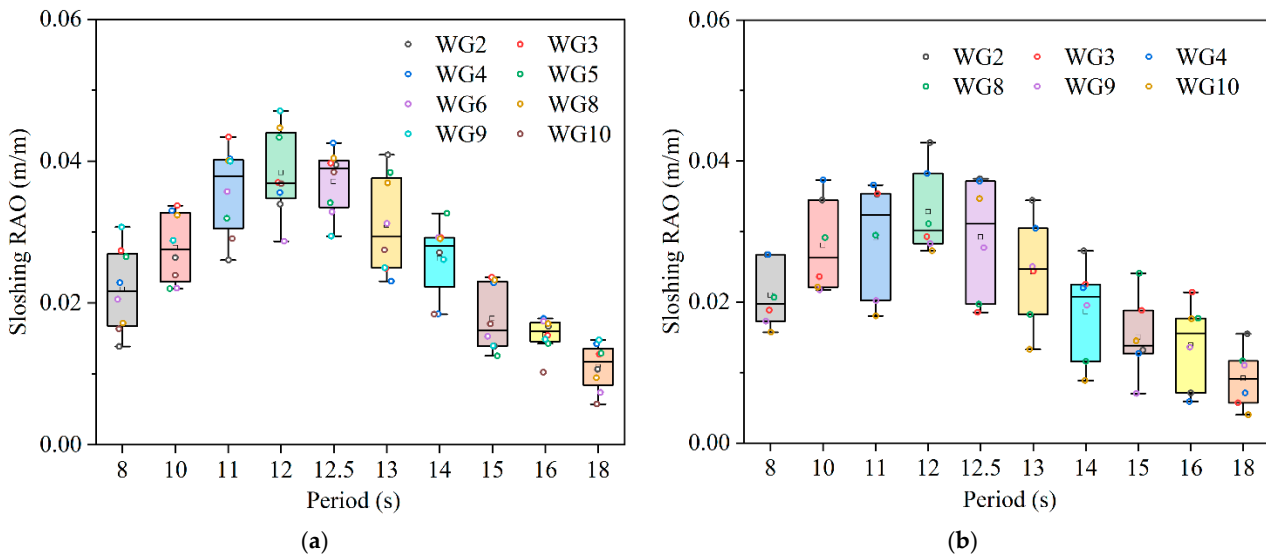


Figure 15. Wave frequency sloshing RAO under head wave condition. (a) Full load; (b) Half load.

#### 4. Sloshing Response under Irregular Waves

The previous section investigated the response characteristics of the aquaculture vessel under the excitation of linear regular waves with a specific period range, whereas the waves encountered during the actual operation are extremely irregular, and this chapter investigates the sloshing response of the aquaculture vessel under the designed extreme operating sea conditions. Similar to the regular wave response study, this chapter considers two typical loading conditions, full and half load, and two typical wave directions, beam and heading sea.

##### 4.1. Irregular Wave Condition

The design limit operating sea state of the aquaculture vessels is a significant wave height ( $H_{1/3}$ ) of 5.8 m, with a peak period ( $T_p$ ) of 12 s. The wave spectrum is selected as the JONSWAP spectrum [47].

$$S(\omega) = \frac{5}{16} (1 - 0.287 \ln(\gamma)) \cdot \frac{H_{1/3}^2 \omega_p^4}{\omega^5} \exp\left(-\frac{5}{4} \left(\frac{\omega}{\omega_p}\right)^{-4}\right) \cdot \gamma \exp(-0.5(\frac{\omega - \omega_p}{\sigma \omega_p})) \quad (2)$$

where  $\omega_p = 2\pi/T_p$  is the angular spectral peak frequency,  $\gamma$  is the non-dimensional peak shape parameter,  $\sigma$  is the spectral width parameter, and  $\sigma = \begin{cases} 0.07 & \text{for } \omega \leq \omega_p \\ 0.09 & \text{for } \omega > \omega_p \end{cases}$ .

To minimize the effect of wave reflection in a single long-duration irregular wave test, multiple short-duration tests with different random seed numbers were re-ran, which makes the total effective duration of the irregular wave longer than 3 h at full scale. The irregular wave was calibrated before the test, and the significant wave height varied from the design value by a maximum of 2.5%, with a maximum variation of the spectral peak period of 6.56%.

Since there are large differences in the amplitude and nonlinearity of the sloshing response under the beam and head seas, the sloshing response of the two wave directions is analyzed independently.

##### 4.2. Beam Wave Condition

The sloshing time history and response spectrum of wave gauges WG1–WG3 at the stern of the aquaculture vessel under full load are shown in Figure 16. The maximum and minimum sloshing amplitude of WG1 are 1.72 m and  $-1.66$  m, respectively, and the range of the sloshing response (deviation between maximum and minimum) is 3.38 m, which is

larger than 2.90 m of WG2 and 3.15 m of WG3. In the extreme operational sea state, the sloshing response was dominated by the wave frequency mode, but a significant first to third natural mode appeared. The amplitude of first natural mode is about 1/3 of the wave frequency mode, and for high natural modes, the amplitude of the modes decreases as the order of the natural modes increases.

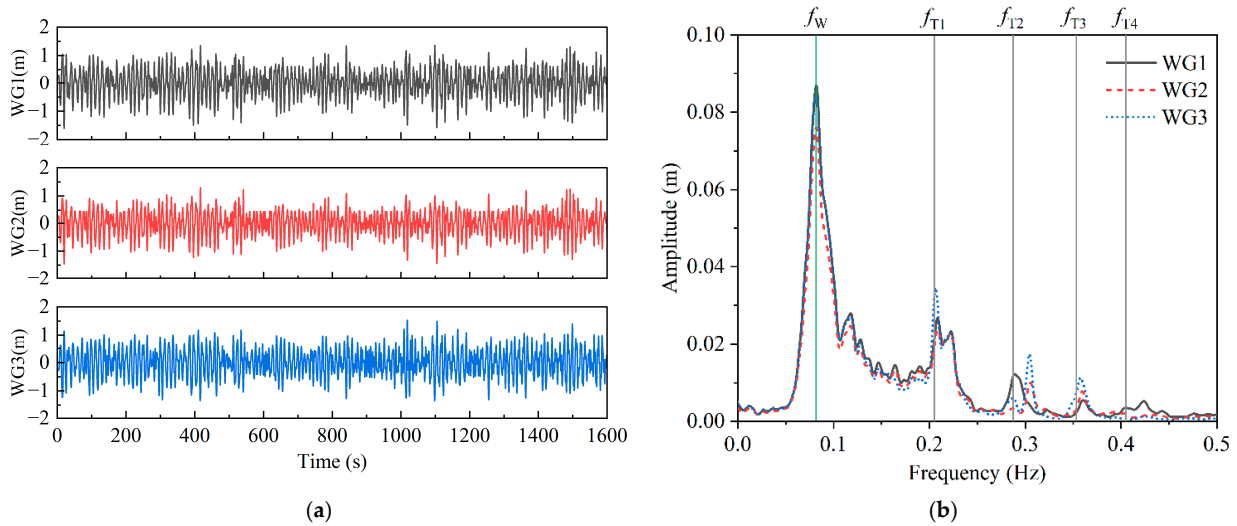


**Figure 16.** Sloshing response and response spectrum under full load and irregular beam wave condition. (a) Sloshing response; (b) Response spectrum.

The typical free surface of the No.1 aquaculture tank without a walkway under the beam wave and full load condition is shown in Figure 17, and the upwelling process at the walkway connection of the tank No.2 is shown in Figure 18. The free surface in tank No.1 showed a large elevation at the side bulkheads, and the free surface was nearly in a planar state. In this condition, the sloshing response can be considered as a quasi-static adjustment process of the static water surface in the tank in response to the hull’s heeling. Figure 18 demonstrates a typical upwelling and receding process at the walkway connection. The superposition of transverse and longitudinal sloshing at the side chamfer of the tank walls and a narrowed angled walkway support plate can cause greater wave upwelling. Both transverse and longitudinal sloshing are superimposed at the corners of the aquaculture tanks, and the narrowing of the upper part of the two adjacent walkways accelerates the upwelling, with jets appearing in the upper gaps (Figure 18IV,V). For the entire test, free liquid level observations revealed that there was no impact on the roofs of the aquaculture tank Nos.1–2.

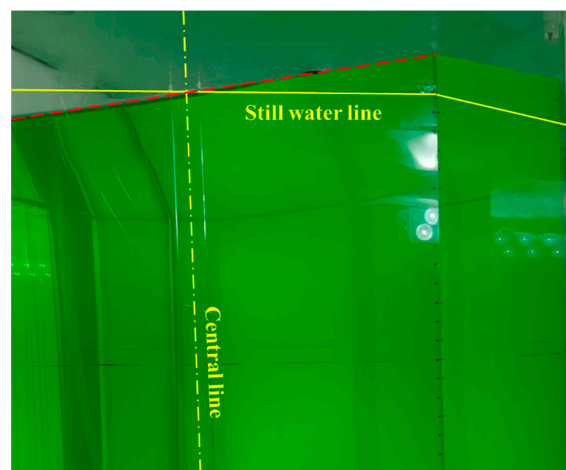


**Figure 17.** Free surface of tank No.1. Red line: transient free surface at the tank wall.

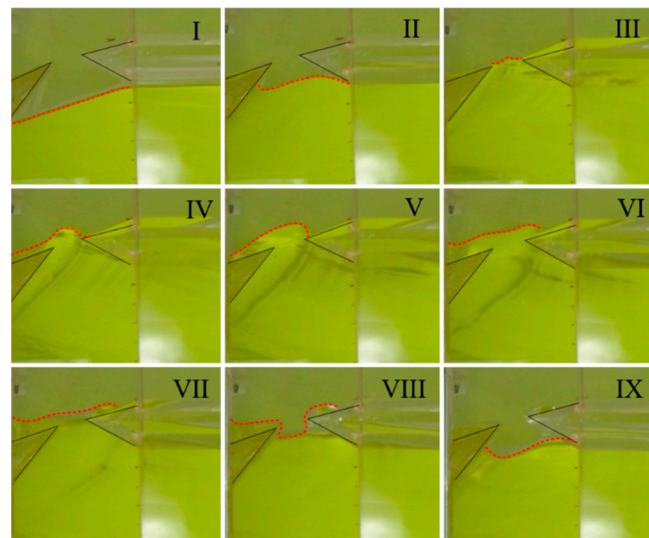


**Figure 18.** Upwelling process at the walkway connection of tank No.2. The black line is the end of the walkway and the red line is the transient free surface at the tank wall. The free surface begins at the design waterline (I), gradually rises to the top of the walkway (II–III), further causing a localized upsurging swell at the walkway connection (IV–V), and then stays briefly on the walkway (VI–VII) and finally begins to fall (VIII–IX).

The sloshing time history and response spectrum of WG1–WG3 under the half load and beam wave condition are shown in Figure 19. The maximum and minimum sloshing amplitude of WG1 are 2.27 m and  $-2.35$  m, respectively, and the range of the sloshing response is 4.62 m, which is larger than 4.18 m of WG2 and 3.66 m of WG3. Significant higher natural modes were observed in the aquaculture tank at the half load condition, particularly the amplitude of first and second natural modes ( $f_{T1}$  and  $f_{T2}$ ) were close to the wave frequency mode, and this large second natural mode was not found in the regular wave test. Since the sloshing response in this state is relatively violent, the sloshing is presented as a three-dimensional (3D) pattern, which further leads to notable first and second natural modes ( $f_{L1}$  and  $f_{L2}$ ) of longitudinal sloshing of WG2 and WG3 as well. On the other hand, in the regular wave test, the doubling frequency mode can be observed for a specific period range of waves, but it is not significant in the irregular response spectrum.

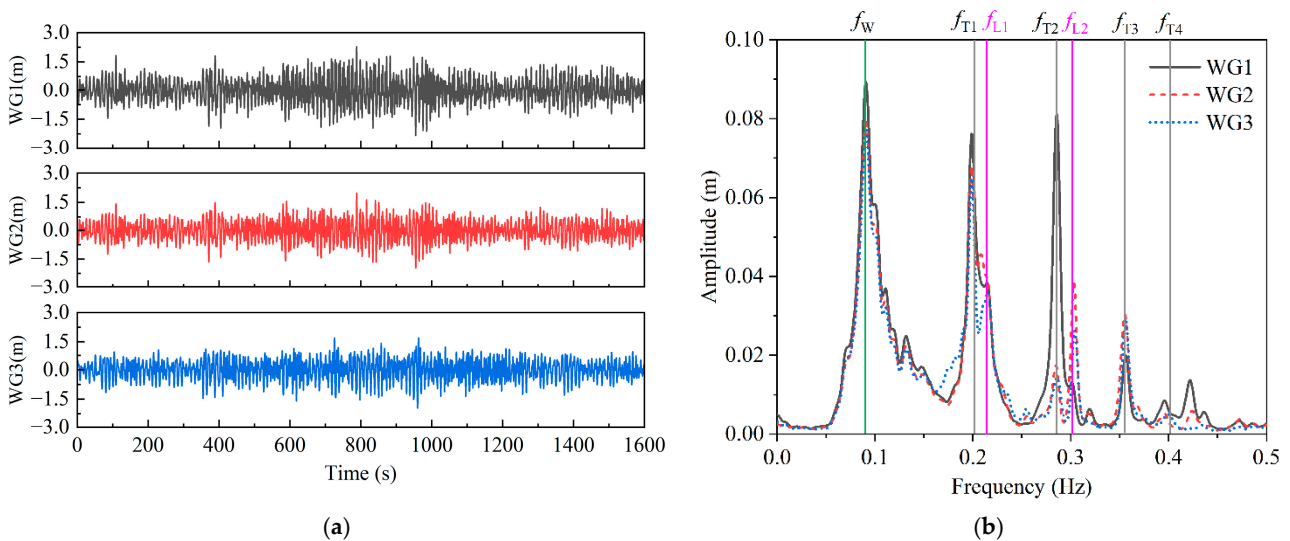


**Figure 19.** Sloshing response and response spectrum under half load and irregular beam irregular wave condition. (a) Sloshing response; (b) Response spectrum.

When comparing the spectrum of the starting stable stage and the later stage of the sloshing response in the regular wave test, it was found that the later stage sloshing response showed a higher natural mode, and the amplitude of the higher natural mode was also larger than that of the starting stable stage. The duration of a single regular wave test is about 45 s–80 s, while a single irregular wave test is about 300 s, which is much longer than that of a regular wave test. On the other hand, the wave height of the irregular wave test is also much larger than that of the regular wave, so the irregular wave test is more likely to evolve to higher natural modes, and the higher natural modes are also excited for a sufficient time, and the amplitude will also increase.

By observing the waveshape in the irregular wave test, it is found that at the start stage when the vessel just encountered the wave, the sloshing response is dominated by the wave frequency mode and first natural mode, and with the growth of the encounter time, the second natural mode appeared, and finally, mixed higher natural modes appeared and formed the 3D standing waves, and the typical evolution of the free surface is shown in Figure 20.

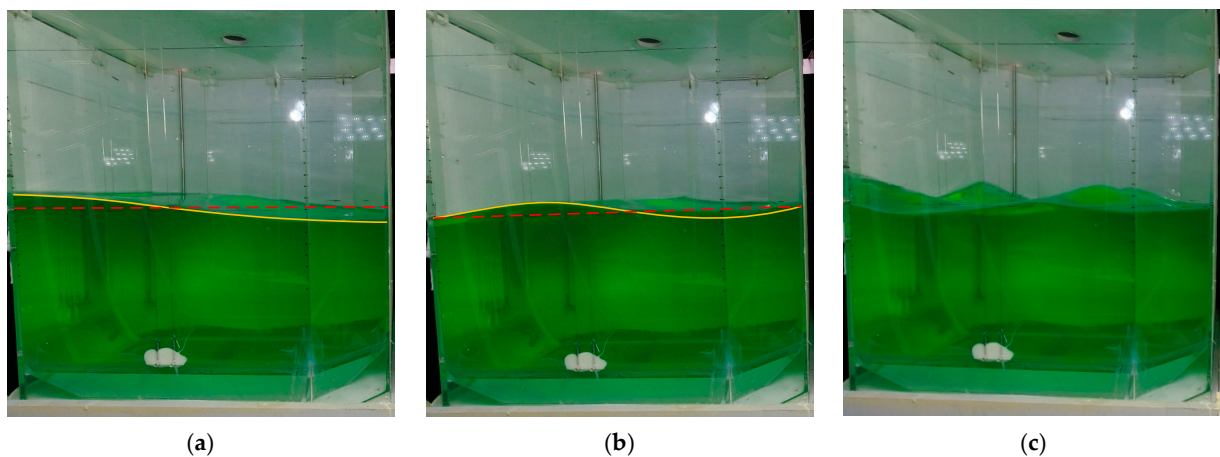


**Figure 20.** Typical evolution of the free surface under half load and beam wave condition. (a) First natural mode; (b) Second natural mode; (c) 3D standing waves. Red lines: the still water line; Yellow lines: the transient free surface at the tank wall.

#### 4.3. Head Wave Condition

The sloshing time history and response spectrum of wave gauges WG1–WG3 under the half load and beam wave condition are shown in Figure 21. WG3 has the largest sloshing amplitude with maximum and minimum values of 0.17 m and  $-0.25$  m, respectively. The sloshing amplitude of WG2 is slightly smaller than WG3, whereas the sloshing amplitude of WG1 is much smaller than the other two wave gauges. The wave frequency mode dominates the longitudinal sloshing in the full load condition, and the amplitude of the first natural mode of WG2 and WG3 is around 1/4 that of the wave frequency mode.

The sloshing time history and response spectrum of WG1–WG3 under the half load and head wave condition are shown in Figure 22. WG2 has the largest sloshing amplitude with maximum and minimum values of 0.22 m and  $-0.25$  m, respectively. The sloshing amplitude of WG3 is slightly smaller than WG2. Similar to the full load condition, the wave frequency mode dominates the longitudinal sloshing in the half load condition. The sloshing response spectrum has a significant first natural frequency of the longitudinal sloshing ( $f_{L1}$ ) of WG2 and WG3. The first and second natural modes ( $f_{L1}$  and  $f_{L2}$ ) in the half load condition are bigger than those in the full load condition.

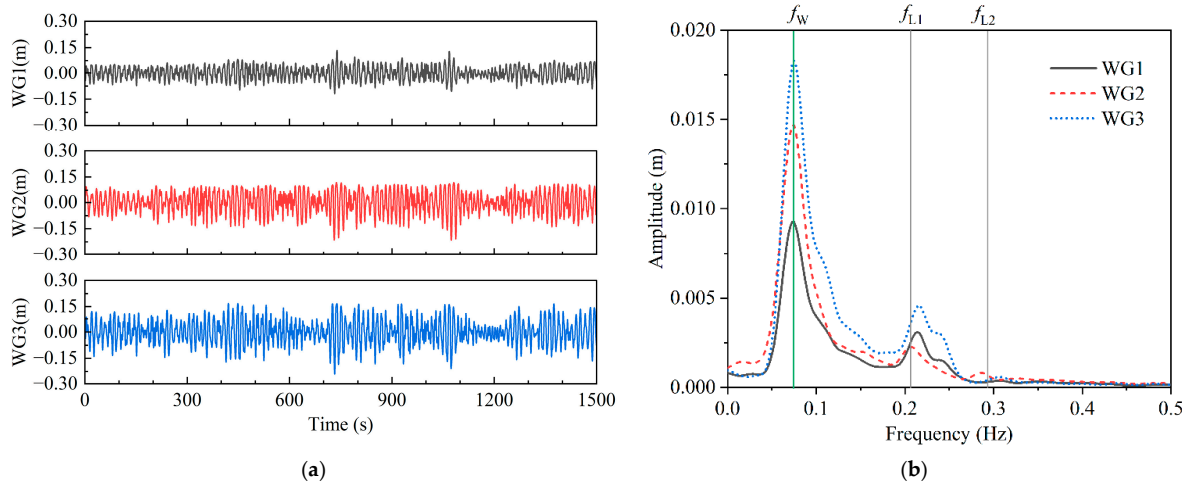


**Figure 21.** Sloshing response and response spectrum under full load and irregular head irregular wave condition. (a) Sloshing response; (b) Response spectrum.

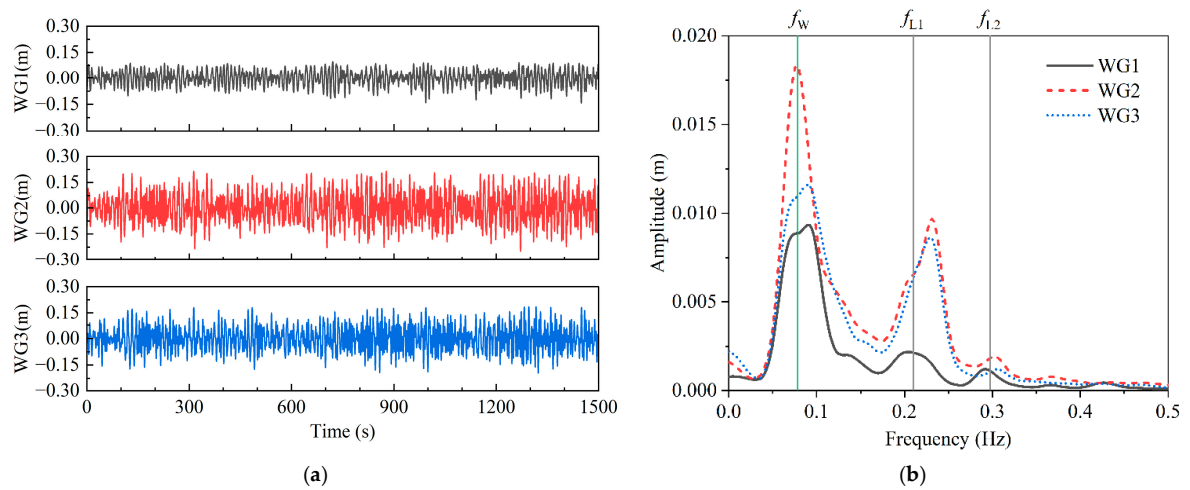


**Figure 22.** Sloshing response and response spectrum under half load and irregular head wave condition. (a) Sloshing response; (b) Response spectrum.

Typical free liquid surface shapes for the full and half load conditions are shown in Figure 23, where the free surface is plate-like for the full load condition and a weaker first natural mode appears on the half load condition.

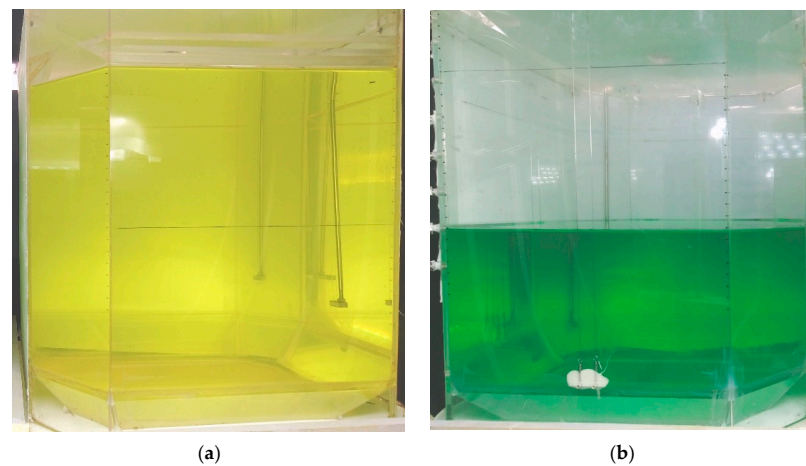


**Figure 23.** Typical free surface shape under head wave condition. (a) Full load; (b) Half load.

## 5. Conclusions

The sloshing response of an aquaculture vessel coupled with external waves is investigated in this study using the experimental method, with two typical filling levels and two wave directions. The frequency domain response characteristics of the sloshing under linear regular waves are analyzed in the regular wave test, and the statistical and frequency domain characteristics of the aquaculture tanks under the limiting sea state are investigated in the irregular wave test. The main conclusions are as follows:

1. In regular wave conditions, the sloshing response is dominated by the wave frequency mode on the whole, except for the case of the wave period of 10 s under the beam wave and half load condition. For the beam wave condition, the wave frequency sloshing has a maximum value when the wave period is close to the roll natural period, meanwhile, the peak of wave frequency sloshing mode in the half load condition is slightly larger than that in the full load condition. For the heading wave condition, the wave frequency sloshing mode is larger when the wave period is about 10 s to 13 s, and at this time, the wave frequency sloshing mode of the half load condition is close to that of the full load condition. The double-row tank arrangement of the vessel can reduce the breadth of the aquaculture tank, so that the first natural period of the tank deviates from the roll and pitch natural period of the hull, and the first resonance phenomenon can be better avoided. This arrangement concept is a useful scheme for the design of similar aquaculture equipment.
2. In regular wave conditions, with a wave period of 10 s, there is a significant first natural mode since the wave period is almost twice the first natural period. Particularly in the beam wave and half load condition, the amplitude of the first natural mode is around three times the wave frequency mode. In the extreme operational sea state, two times the first natural period is in the main energy range of the irregular waves, which likewise causes a more significant first natural response.
3. In the extreme sea state, the sloshing amplitude in the beam wave condition is about 7–10 times that of the head wave condition at the same filling level. The sloshing amplitude in the half load condition is 1.4 and 1.15 times that of the full load state for the beam wave and head wave condition, respectively. Therefore, a half load condition should be avoided during the culture operation, and in addition, the designer can enlarge the designed water depth in the aquaculture tank to increase the filling level. Green water occurred on the roof of the walkway in the beam wave conditions but did not impact the roof of the aquaculture tanks. In this case, personnel should not be allowed to enter the tank for culture operations, while the designer needs to pay attention to the impact loads of the walkway. Complex 3D standing waves with first and second natural modes of transverse and longitudinal sloshing were observed under the beam wave and half load conditions. Operationally, aquaculture vessels should choose an appropriate mooring scheme or sail autonomously away from typhoons to avoid harsh beam seas.
4. The nonlinearity of the sloshing response is much stronger in the extreme sea state than in the regular wave at the same filling level and wave direction, and the sloshing response in the extreme sea state has higher natural modes, particularly a significant fourth natural mode in beam wave and half load conditions. The proportion of higher natural modes to wave frequency modes has increased as well. This is owing to the irregular wave test having a long duration, which is more likely to trigger higher natural modes, and the higher natural modes evolved over enough time to increase in amplitude.

In the present study, the sloshing response was studied using the experimental method, as a comparison, the numerical simulations are also being studied, which will be reported later separately. Furthermore, the impact loads caused by sloshing and the flow pattern of the aquaculture tanks are being investigated, both of which are important for the design of the aquaculture vessels.

**Author Contributions:** Data curation, Y.T., Q.W. and F.H.; funding acquisition, R.Z. and J.G.; investigation, Z.Z. and X.X.; methodology, Z.Z. and X.X.; supervision, R.Z. and J.G.; writing—original draft, Y.T.; Conceptualizing, Z.L. All authors have read and agreed to the published version of the manuscript.

**Funding:** This work was supported by the National Natural Science Foundation of China [Grant No. 52271318].

**Institutional Review Board Statement:** Not applicable.

**Informed Consent Statement:** Not applicable.

**Data Availability Statement:** Data are contained within the article.

**Acknowledgments:** The authors acknowledge the meticulous test adjustment and data collection work of Weifa Liu at Guangzhou Salvage Bureau of the Ministry of Transport and Tengjiao Sang at AVIC Special Vehicle Research Institute of China.

**Conflicts of Interest:** The authors declare no conflict of interest.

### Abbreviations

NO <sub>x</sub>	Nitrogen oxides
RANS	Reynolds averaged Navier–Stokes
CIP	Constraint interpolation profile
SPH	Smoothed Particle Hydrodynamics
BL	Base line
AP	After perpendicular
WG	Wave gauge
AVIC	Aviation Industry Corporation
FPSO	Floating production storage and offloading unit
ITTC	International Towing Tank Conference
RAO	Response amplitude operator
JONSWAP	Joint North Sea Wave Project

### References

1. FAO. *The State of World Fisheries and Aquaculture 2022. Towards Blue Transformation*; FAO: Rome, Italy, 2022; p. 266.
2. DNV. *Oceans' Future to 2050: Marine Aquaculture Forecast*; DNV: Høvik, Norway, 2021; p. 48.
3. Zhao, Y.P.; Guan, C.T.; Bi, C.W.; Liu, H.F.; Cui, Y. Experimental Investigations on Hydrodynamic Responses of a Semi-Submersible Offshore Fish Farm in Waves. *J. Mar. Sci. Eng.* **2019**, *7*, 238. [\[CrossRef\]](#)
4. Shen, Y.G.; Firoozkoobi, R.; Greco, M.; Faltinsen, O.M. Comparative investigation: Closed versus semi-closed vertical cylinder-shaped fish cage in waves. *Ocean Eng.* **2022**, *245*, 110397. [\[CrossRef\]](#)
5. Li, L.; Jiang, Z.; Vangdal Høiland, A.; Chen Ong, M. Numerical Analysis of a Vessel-Shaped Offshore Fish Farm. *J. Offshore Mech. Arct. Eng.* **2018**, *140*, 041201. [\[CrossRef\]](#)
6. Chu, Y.I.; Wang, C.M. Hydrodynamic Response Analysis of Combined Spar Wind Turbine and Fish Cage for Offshore Fish Farms. *Int. J. Struct. Stab. Dyn.* **2020**, *20*, 2050104. [\[CrossRef\]](#)
7. Li, Z.; Guo, X.; Cui, M. Numerical investigation of flow characteristics in a rearing tank aboard an aquaculture vessel. *Aquac. Eng.* **2022**, *98*, 102272. [\[CrossRef\]](#)
8. Zheng, J.H.; Xue, M.A.; Dou, P.; He, Y.M. A review on liquid sloshing hydrodynamics. *J. Hydrodyn.* **2021**, *33*, 1089–1104. [\[CrossRef\]](#)
9. Faltinsen, O.M.; Rognebakke, O.F.; Timokha, A.N. Resonant three-dimensional nonlinear sloshing in a square-base basin. *J. Fluid Mech.* **2003**, *487*, 1–42. [\[CrossRef\]](#)
10. Lugni, C.; Brocchini, M.; Faltinsen, O.M. Wave impact loads: The role of the flip-through. *Phys. Fluids* **2006**, *18*, 122101. [\[CrossRef\]](#)
11. Souto-Iglesias, A.; Botia-Vera, E.; Martín, A.; Pérez-Arribas, F. A set of canonical problems in sloshing. Part 0: Experimental setup and data processing. *Ocean Eng.* **2011**, *38*, 1823–1830. [\[CrossRef\]](#)
12. Zhu, R.Q.; Wu, Y.S. A Numerical Study on Sloshing Phenomena in a Liquid Tank. *Shipbuild. China* **2002**, *43*, 17–23.
13. Chen, Y.; Xue, M.-A. Numerical Simulation of Liquid Sloshing with Different Filling Levels Using OpenFOAM and Experimental Validation. *Water* **2018**, *10*, 1752. [\[CrossRef\]](#)
14. Sanchez-Mondragon, J.; Felix-Gonzalez, I.; Cruces-Giron, A.R. Turbulence analysis for vertical baffle configurations on prismatic tanks by the MPS method. *Ocean Eng.* **2022**, *264*, 112392. [\[CrossRef\]](#)
15. Zhang, Y.X.; Wan, D.C.; Hino, T. Comparative study of MPS method and level-set method for sloshing flows. *J. Hydrodyn. Ser. B* **2014**, *26*, 577–585. [\[CrossRef\]](#)
16. Cao, X.Y.; Ming, F.R.; Zhang, A.M. Sloshing in a rectangular tank based on SPH simulation. *Appl. Ocean Res.* **2014**, *47*, 241–254. [\[CrossRef\]](#)

17. Rognebakke, O.F.; Faltinsen, O.M. Coupling of Sloshing and Ship Motions. *J. Ship Res.* **2003**, *47*, 208–221. [[CrossRef](#)]
18. Newman, J.N. Wave effects on vessels with internal tanks. In Proceedings of the 20th International Workshop on Water Waves and Floating Bodies, Svalbard, Norway, 29 May–1 June 2005.
19. Martić, I.; Degiuli, N.; Catipović, I. Evaluation of the added resistance and ship motions coupled with sloshing using potential flow theory. *Brodogradnja* **2016**, *67*, 109–122. [[CrossRef](#)]
20. Lee, D.Y.; Choi, H.S.; Faltinsen, O.M. A study on the sloshing effect on the motion of 2d boxes in regular waves. *J. Hydrodyn.* **2010**, *22*, 429–434. [[CrossRef](#)]
21. Nam, B.-W.; Kim, Y.; Kim, D.-W.; Kim, Y.-S. Experimental and numerical studies on ship motion responses coupled with sloshing in waves. *J. Ship Res.* **2009**, *53*, 68–82. [[CrossRef](#)]
22. Chen, B.F.; Chiang, H.W. Complete two-dimensional analysis of sea-wave-induced fully non-linear sloshing fluid in a rigid floating tank. *Ocean Eng.* **2000**, *27*, 953–977. [[CrossRef](#)]
23. Zhao, D.; Hu, Z.; Chen, G.; Chen, X.; Feng, X. Coupling analysis between vessel motion and internal nonlinear sloshing for FLNG applications. *J. Fluids Struct.* **2018**, *76*, 431–453. [[CrossRef](#)]
24. Su, Y.; Liu, Z.Y. Coupling effects of barge motion and sloshing. *Ocean Eng.* **2017**, *140*, 352–360. [[CrossRef](#)]
25. Xiao, K.L.; Chen, Z.G.; Dai, Y. Numerical Study on Coupling Effect of Multi-tank Sloshing and Ship Motion. *Ship Eng.* **2020**, *42*, 50–54. [[CrossRef](#)]
26. Zhuang, Y.; Yin, C.; Wan, D. Numerical study on coupling effect of LNG tank sloshing and ship motion in wave. In Proceedings of the The Eleven Asian Computational Fluid Dynamics Conference (ACFD11), Dalian, China, 16–20 September 2016; pp. 432–436.
27. Liu, L.W.; Feng, D.K.; Wang, X.Z.; Zhang, Z.G.; Yu, J.W.; Chen, M.X. Numerical study on the effect of sloshing on ship parametric roll. *Ocean Eng.* **2022**, *247*, 110612. [[CrossRef](#)]
28. Zhao, W.; Yang, J.; Tao, L.; White, D. Research on the Coupling Effects Between Ship Motions and Sloshing. In Proceedings of the ASME 2014 33rd International Conference on Ocean, Offshore and Arctic Engineering, San Francisco, CA, USA, 8–13 June 2014.
29. Kim, Y.; Nam, B.W.; Kim, D.W.; Kim, Y.S. Study on coupling effects of ship motion and sloshing. *Ocean Eng.* **2007**, *34*, 2176–2187. [[CrossRef](#)]
30. Zhao, W.; Taylor, P.H.; Wolgamot, H.A.; Eatock Taylor, R. Identifying linear and nonlinear coupling between fluid sloshing in tanks, roll of a barge and external free-surface waves. *J. Fluid Mech.* **2018**, *844*, 403–434. [[CrossRef](#)]
31. Igbadumhe, J.F.; Bonoli, J.; Dzielski, J.; Furth, M. Coupled FPSO roll motion response and tank sloshing in a pair of two row cargo tanks. *Ocean Eng.* **2023**, *278*, 114273. [[CrossRef](#)]
32. Li, H.; Sun, Z.Y.; Han, B.B.; Shao, Y.H.; Deng, B.L. Research on the motion response of aquaculture ship and tank sloshing under rolling response. *Brodogradnja* **2022**, *73*, 1–15. [[CrossRef](#)]
33. Neves, M.A.S.; Merino, J.A.; Rodríguez, C.A. A nonlinear model of parametric rolling stabilization by anti-roll tanks. *Ocean Eng.* **2009**, *36*, 1048–1059. [[CrossRef](#)]
34. Dou, P.; Xue, M.-A.; Zheng, J.; Zhang, C.; Qian, L. Numerical and experimental study of tuned liquid damper effects on suppressing nonlinear vibration of elastic supporting structural platform. *Nonlinear Dyn.* **2020**, *99*, 2675–2691. [[CrossRef](#)]
35. Jithu, S.; Janardhanan, S.; Asok, N. Numerical Study on the Effect of Ball Baffles in Reducing Sloshing Loads in Ship Tanks. In Proceedings of the International Conference on Computational and Experimental Marine Hydrodynamics, Chennai, India, 25–27 November 2018.
36. Kim, T.W.; Kim, S.K.; Park, S.B.; Lee, J.M. Design of Independent Type-B LNG Fuel Tank: Comparative Study between Finite Element Analysis and International Guidance. *Adv. Mater. Sci. Eng.* **2018**, *2018*, 5734172. [[CrossRef](#)]
37. Trimulyono, A.; Athariq, H.; Chrismianto, D.; Samuel, S. Investigation of sloshing in the prismatic tank with vertical and T-shape baffles. *Brodogradnja* **2022**, *73*, 43–58. [[CrossRef](#)]
38. Yu, Y.M.; Ma, N.; Fan, S.M.; Gu, X.C. Experimental and numerical studies on sloshing in a membrane-type LNG tank with two floating plates. *Ocean Eng.* **2017**, *129*, 217–227. [[CrossRef](#)]
39. Koh, C.G.; Luo, M.; Gao, M.; Bai, W. Modelling of liquid sloshing with constrained floating baffle. *Comput. Struct.* **2013**, *122*, 270–279. [[CrossRef](#)]
40. Cui, M.; Li, Z.; Zhang, C.; Guo, X. Statistical investigation into the flow field of closed aquaculture tanks aboard a platform under periodic oscillation. *Ocean Eng.* **2022**, *248*, 110677. [[CrossRef](#)]
41. Gao, R.; Cui, M.C.; Wang, Q.W.; Wang, J. Numerical Analysis on Roll Fish-suitability of Aquaculture Water Tank. *Ship Eng.* **2020**, *42*, 35–47. [[CrossRef](#)]
42. Wiegerink, J.J.; Baldock, T.E.; Callaghan, D.P.; Wang, C.M. Experimental study on hydrodynamic response of a floating rigid fish tank model with slosh suppression blocks. *Ocean Eng.* **2023**, *273*, 113772. [[CrossRef](#)]
43. Tao, Y.W.; Zhu, R.Q.; Gu, J.Y.; Li, Z.Y.; Zhang, Z.Y.; Xu, X.S. Experimental and numerical investigation of the hydrodynamic response of an aquaculture vessel. *Ocean Eng.* **2023**, *279*, 114505. [[CrossRef](#)]
44. ITTC. Recommended Procedures and Guidelines: Ship Models. 2017, 7.5-01-01-01. Available online: <https://www.ittc.info/media/9571/75-01-01-01.pdf> (accessed on 6 October 2023).
45. ITTC. Recommended Procedures and Guidelines: Seakeeping Experiments. 2017, 7.5-02-07-02.1. Available online: <https://www.ittc.info/media/9705/75-02-07-021.pdf> (accessed on 6 October 2023).

46. ITTC. Recommended Procedures and Guidelines: Sloshing Model Tests. 2021, 7.5-02-07-02.7. Available online: <https://www.itc.info/media/9715/75-02-07-027.pdf> (accessed on 6 October 2023).
47. DNV. *Environmental Conditions and Environmental Loads*; DNV: Høvik, Norway, 2014; DNV-RP-C205, 182. Available online: <https://www.dnv.com/rules-standards/index.html> (accessed on 6 October 2023).

**Disclaimer/Publisher’s Note:** The statements, opinions and data contained in all publications are solely those of the individual author(s) and contributor(s) and not of MDPI and/or the editor(s). MDPI and/or the editor(s) disclaim responsibility for any injury to people or property resulting from any ideas, methods, instructions or products referred to in the content.